Applied Physics A (2020) 126:652
https://doi.org/10.1007/s00339-020-03846-2

Applied Physics A
Materials Science & Processing

Interfacial transfer and phase evolution between Cu and Sn solder doped with minor Cu, Ag and Ni: experimental and theoretical investigations

Mingyuan Yang[1] · Jieshi Chen[1,2,4] · Jin Yang[1,2] · Peilei Zhang[1,2] · Zhishui Yu[1,2] · Zhi Zeng[3] · Hao Lu[4]

Received: 9 June 2020 / Accepted: 23 July 2020 / Published online: 31 July 2020

Abstract
The effects of minor Cu (0.7%), Ag (3.5%) and Ni (0.1%) additions in Sn solder on the interfacial transfer and phase evolution were clarified in Sn/Cu solder joints. $(Cu,M)_6Sn_5$ and $(Cu,M)_3Sn$ (M = Cu, Ni) layers were observed at the Sn/Cu interface during thermal aging at 150 °C. The additions of Cu, Ag and Ni alloy elements were found to change the growth of the Cn–Sn intermetallic compounds (IMCs). The results showed that Cu, Ag and Ni additions were able to suppress the growth of $(Cu,M)_3Sn$ (M = Cu, Ni) layers, but promoted the $(Cu,M)_6Sn_5$ growth. This was because the reactions on the $(Cu,M)_6Sn_5$ side were promoted by the refined IMCs grain size, whose growth was at the expense of $(Cu,M)_3Sn$. In addition, the interfacial transfer rate (thickness ratio, y) of $(Cu,M)_3Sn/(Cu,M)_6Sn_5$ versus the thermal aging time (t) was found to be close to parabola relationship, the y increased gradually with the alloy elements from Ni, Cu to Ag. The phase evolution (η'-Cu_6Sn_5, η-Cu_6Sn_5, ε-Cu_3Sn, Ag_3Sn, η'-$(Cu,Ni)_6Sn_5$, η-$(Cu,Ni)_6Sn_5$ and ε-$(Cu,Ni)_3Sn$) at the interface between Cu and Sn solder doped with minor Cu, Ag and Ni was also elucidated.

Keywords Solder · Interfacial transfer · Phase evolution · Diffusion · Element addition

1 Introduction

With the rapid development of mobile electronic devices, higher requirements and challenges are imposed on electronic packaging technology [1–3]. Sn-based solder is the main material for electronic packaging. The Sn-based solder in the solder joint reacts with the substrate metal during the soldering process and is converted into intermetallic compounds (IMCs). During the subsequent service of the solder joint, the IMCs at the interface will further grow and transform [4–6]. To better interconnect the solder joints, a uniform thickness of the IMCs layer is necessary, but the IMCs layer may cause cracking of the interconnect interface due to brittleness, resulting in solder joint failure [7–9]. Therefore, the IMCs layer acts as the only interconnect medium, and its reliability and service performance play a decisive role [10–13].

In Sn–Cu solder joints, when the molten Sn-based solder alloy the Cu, Cu_6Sn_5 and Cu_3Sn IMCs form at the solder/Cu interface. It was reported that adding minor alloying elements into the solder reduced the unbalanced diffusion of Cu and Sn, suppressing the formation of the IMCs layer and reducing the brittleness of the joint [14–16]. For example, trace Zn [17, 18], Fe [19], Co [19] and Ni [19, 20] were separately added into the solder to retard the formation and growth of Cu_3Sn layer. Cu and Ag were basic elements in the lead-free solder. The addition of Cu reduced the concentration gradient of Cu and suppressed the growth of the Cu_3Sn layer [21]. The Sn3.5Ag/Cu solder joints led to a local enrichment of Ag at the interface and promoted the formation of large Ag_3Sn IMCs via the Cu_6Sn_5 heterogeneous

✉ Jieshi Chen
cjshbb@sjtu.edu.cn

✉ Zhi Zeng
zhizeng@uestc.edu.cn

[1] School of Materials Engineering, Shanghai University of Engineering Science, Shanghai 201602, China

[2] Shanghai Collaborative Innovation Center of Laser Advanced Manufacturing Technology, Shanghai 201620, China

[3] School of Mechanical and Electrical Engineering, University of Electronic Science and Technology of China, Chengdu 611731, China

[4] School of Materials Science and Engineering, Shanghai Jiao Tong University, Shanghai 200240, China

nucleation sites [22]. The plate-like Ag_3Sn affected the growth and morphology of Cu_6Sn_5 layer and the stability of the solder joint [23, 24]. In addition, one of the more noteworthy alloying elements was Ni. It was shown Ni addition to Sn3.5Ag (3.5 wt% Ag, balance Sn) in amounts as minute as 0.1 wt% could substantially hinder the Cu_3Sn growth during soldering as well as during the following solid-state aging [25]. The Cu_3Sn growth was linked to the formation of micro voids, which in turn increased the potential for brittle interfacial fracture [26]. It was shown that drop test performance increased for solder joints with just a small amount of Ni addition [27]. However, the sensitivity of interfacial transfer in solder/Cu interface by considering minor Cu, Ag and Ni was not completely clear. Especially, the influence of Cu, Ag and Ni addition on the fluxes of Cu and Sn atom diffusion in solder/Cu interface needs more detailed explanations. Moreover, the phase of η'-Cu_6Sn_5, η-Cu_6Sn_5, ε-Cu_3Sn, Ag_3Sn, η'-$(Cu,Ni)_6Sn_5$, η-$(Cu,Ni)_6Sn_5$ and ε-$(Cu,Ni)_3Sn$ are found at interface between Cu and Sn solder doped with minor Cu, Ag and Ni. The phase evolution needs further clarification, due to the fact that phase transformation dictates the joint reliability.

The objective of this study is to examine the sensitivity of interfacial transfer in solder/Cu interface by considering minor Cu, Ag and Ni. Emphasis is placed on a systematic comparison study on the fluxes of Cu and Sn atom diffusion. Furthermore, the interface evolution, especially the interface phase evolution is discussed.

2 Experimental and theoretical methods

2.1 Experimental procedures

The solders used in this work were pure Sn (99.99%), Sn0.7Cu (wt%), Sn3.5Ag (wt%) and Sn0.1Ni (wt%). The former two were commercially, and Sn3.5Ag (wt%) and Sn0.1Ni (wt%) were fabricated form pure Sn (99.99%) and Ag (99.99%) and Ni (99.99%) using means of smelting, respectively. The high purity Cu foil (99.99%, 10 mm × 10 mm × 0.1 mm) was chose as the substrate. The solder joints were prepared by melting solder on the foils at 260 °C for 1 min, and then the reflowed sample were cooled at a fast cooling rate. To investigate the interfacial microstructure in the solder joints, the isothermal aging for the as-reflowed samples was performed at 150 °C with different aging periods (72 h, 120 h, 240 h, 360 h and 480 h). Then these samples were mounted in epoxy and mechanical polished. The cross-sectional microstructure at the interface was observed by SEM (Sirion200), and the compositions of IMC layer were determined by energy dispersive spectroscopy (EDS).

The average thickness of IMCs layer was measured with the software Image J. The average thickness of the IMCs layer was calculated by dividing the IMCs layer area by the length of the interface. 8–10 SEM images with 1000 magnification were selected to estimate the mean thickness for each sample. To observe the three-dimensional morphology of the interfacial IMCs, the Sn coating was etched completely using a 10% HNO_3 + 90% ethanol solution [28].

2.2 Calculation details

The calculations were carried out using the CASTEP plane-wave code [29] in the scheme of generalized gradient approximation (GGA-PBE) [30]. The Vanderbilt ultrasoft pseudopotentials [31] were employed to treat the valence electrons for Cu ($3d^{10}4s^1$), Sn ($5s^25p^2$), Ag ($4d^{10}5s^1$) and Ni ($3d^84s^2$). Brillouin-zone integrations were performed using Monkhorst and Pack *k*-point meshes [32]. To obtain the most equilibrium crystal structure and to ensure the accuracy of subsequent calculations, convergence tests for the total energy were strictly implemented. For all crystal systems, with the *k*-point meshes fixed at 8 × 12 × 12, we increased the cut-off energy from 350 to 400 eV, and the change in total energy was below 2×10^{-3} eV/atom. Then we fixed the cut-off energy at 350 eV and varied the *k*-point meshes from 4 × 6 × 6 to 8 × 8 × 10, and the change in total energy was less than 10^{-4} eV/atom. Following this rule, the changes in total energy for the other phases were no more than 10^{-2} eV/atom with the change of cut-off energy and *k*-point meshes.

The settings for these calculations are shown in Table 3. The energy cutoff was 350 eV. The convergence tolerance was selected as follows: minimum energy less than 1.0×10^{-5} eV/atom, maximum force less than 0.03 eV Å^{-1}, maximum stress less than 0.05 GPa, and maximum displacement less than 1×10^{-3} Å.

3 Results and discussion

3.1 Interfacial microstructures evolution of Sn–*x*/Cu joints

The interfacial microstructure of Sn–*x*/Cu (*x* = 0, 0.7Cu, 3.5Ag and 0.1Ni) joints after aging at 150 °C with different aging periods were shown in Figs. 1, 2, 3 and 4. In all of the images, the upper, middle and bottom materials were solder alloy, interfacial IMCs layer and Cu pad, respectively. The chemical compositions of the IMCs layers were characterized by EDS analysis and the results are listed in Table 1.

Figure 1a shows the interfacial microstructure of as-reflowed Sn/Cu joint. A layer of scallop-type growth of Cu_6Sn_5 in solid–liquid inter-diffusion reaction [33, 34]. After aging at 150 °C for 120 h, the Cu_3Sn layer was

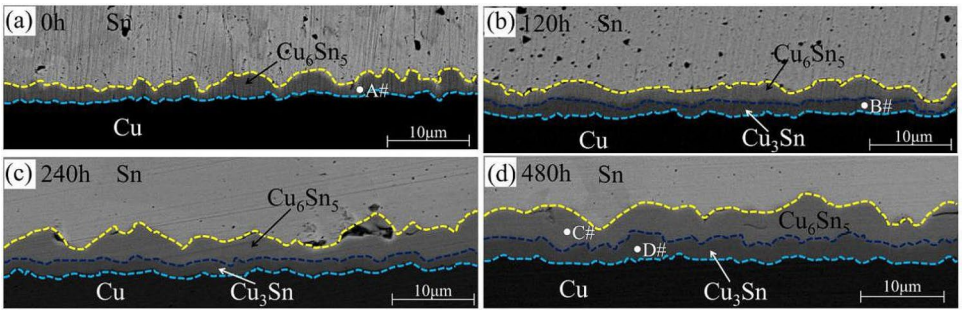

Fig. 1 Cross-sectional BSE images of Sn/Cu joints after aging at 150 °C. **a** 0 h; **b** 120 h; **c** 240 h; **d** 480 h

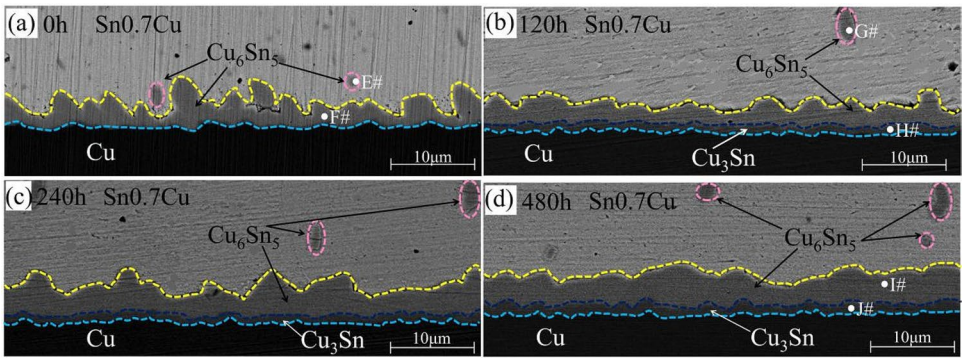

Fig. 2 Cross-sectional BSE images of Sn0.7Cu/Cu joints after aging at 150 °C. **a** 0 h; **b** 120 h; **c** 240 h; **d** 480 h

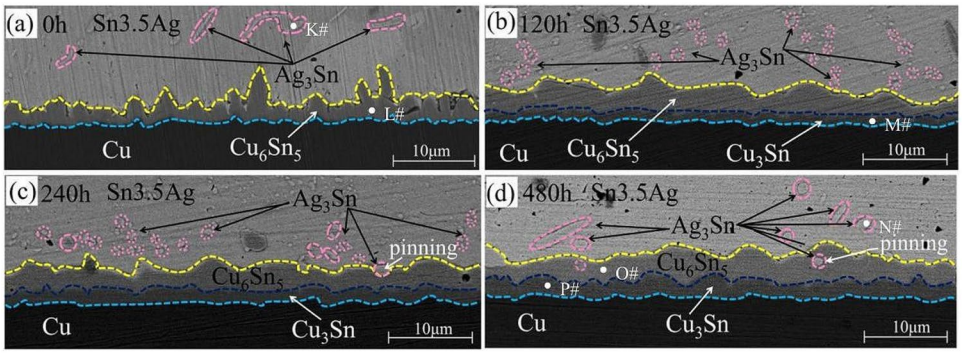

Fig. 3 Cross-sectional BSE images of Sn3.5Ag/Cu joints after aging at 150 °C. **a** 0 h; **b** 120 h; **c** 240 h; **d** 480 h

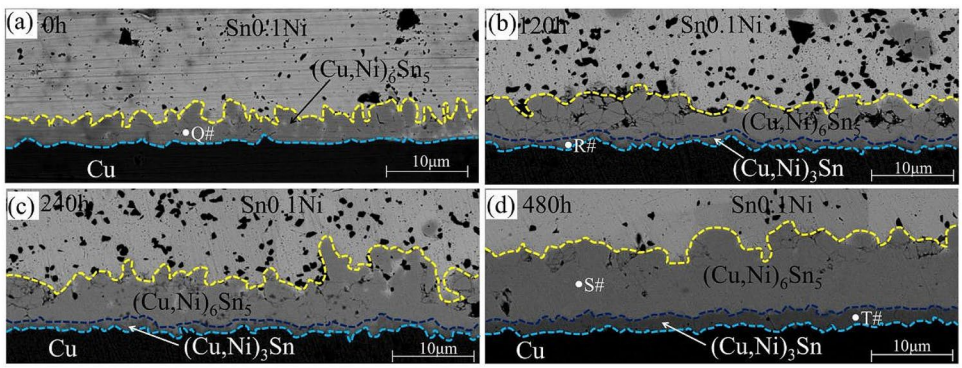

Fig. 4 Cross-sectional BSE images of Sn0.1Ni/Cu joints after aging at 150 °C. **a** 0 h; **b** 120 h; **c** 240 h; **d** 480 h

formed between the Cu_6Sn_5 and Cu layers, as presented in Fig. 1b. After aging time was extended to 240 h, as shown in Fig. 1c, the thickness of Cu_6Sn_5 and Cu_3Sn layers gradually increased in the Sn/Cu joint. When the aging time was further extended to 480 h, as shown in Fig. 1d, the total IMCs thickness in the Sn/Cu joint interface was continuously

Table 1 EDS results of IMCs phase at the interface of Sn–*x*/Cu (*x* = 0, 0.7Cu, 3.5Ag and 0.1Ni) joints in following different thermal aging times

Point	Cu (at%)	Sn (at%)	Phase	Point	Cu (at%)	Sn (at%)	Ag (at%)	Ni (at%)	Phase
A#	58.45	41.55	Cu_6Sn_5	K#	0	25.66	74.34	0	Ag_3Sn
B#	74.38	25.62	Cu_3Sn	L#	54.77	45.23	0	0	Cu_6Sn_5
C#	57.64	42.36	Cu_6Sn_5	M#	75.55	24.45	0	0	Cu_3Sn
D#	73.75	26.25	Cu_3Sn	N#	0	26.23	73.77	0	Ag_3Sn
E#	57.87	42.13	Cu_6Sn_5	O#	56.46	42.54	0	0	Cu_6Sn_5
F#	56.79	43.21	Cu_6Sn_5	P#	76.33	23.67	0	0	Cu_3Sn
G#	55.42	44.58	Cu_6Sn_5	Q#	50.32	45.67	0	4.01	$(Cu,Ni)_6Sn_5$
H#	75.67	24.33	Cu_3Sn	R#	71.46	26.32	0	2.22	$(Cu,Ni)_3Sn$
I#	54.88	45.12	Cu_6Sn_5	S#	51.57	44.76	0	3.67	$(Cu,Ni)_6Sn_5$
J#	75.44	24.56	Cu_3Sn	T#	72.89	24.96	0	2.15	$(Cu,Ni)_3Sn$

thickened, the Cu_6Sn_5 layer increased slightly and Cu_3Sn layer grew much quicker than the Cu_6Sn_5 layer. Moreover, the morphology of IMCs became flattened, because Cu diffusion through the scallop valleys was faster than that through the scallop hills [35].

Figure 2a shows the interfacial microstructures of as-reflowed Sn0.7Cu/Cu joints. Similar to the as-reflowed Sn/Cu joint, a layer of Cu_6Sn_5 was formed at the interface. After a 120 h aging treatment at 150 °C, as shown in Fig. 2b, the IMC layer thickness increased obviously. A thin Cu_3Sn layer emerged between Cu_6Sn_5 and Cu. After aging time was extended to 240 h, the Cu_6Sn_5 layer thickness significantly increased (Fig. 2c). The thickness of Cu_3Sn layer was found to be sensitive to the Cu content. The addition of Cu suppressed growth of Cu_3Sn layer. Figure 2d presents the interfacial microstructures of the solder joints aged at 150 °C for 480 h. It was seen that the IMC layer continued to grow up. However, a thinner Cu_3Sn layer was formed at the Sn0.7Cu/Cu interface than that of Sn/Cu joint.

The interfacial microstructure of as-reflowed Sn3.5Ag/Cu joints is observed in Fig. 3a. Scallop-shaped Cu_6Sn_5 layer was formed at the interface and Ag_3Sn phase was found in Sn3.5Ag solder. After aging at 150 °C for 120 h, the total thickness of IMCs layer gradually increased, and Ag_3Sn phase gradually increased forming a small amount of discrete particle-like phases, as shown in Fig. 3b. After aging time was extended to 240 h, the discrete particle-like Ag_3Sn phase significantly increased. The Cu_6Sn_5 layer thickness increased not obviously, but the thickness of Cu_3Sn layer obviously increased with the rising aging time (Fig. 3c). When the aging time was extended to 480 h, Ag_3Sn phase gradually embedded in grain boundary of IMCs layer, as shown in Fig. 3d. The Ag_3Sn phases acted a pinning effect, which divided the solder substrate into many regions, and affected the unbalanced diffusion of Cu and Sn.

The microstructure evolution of the Sn0.1Ni/Cu joint interface is shown in Fig. 4. As shown in Fig. 4a, it was seen that a new IMCs layer emerged at the Sn0.1Ni/Cu interface. Based on the EDS analysis, this new IMC layer was identified as $(Cu,Ni)_6Sn_5$. It suggested that IMCs layer was found to be sensitive to the Ni content. After aging at 150 °C for 120 h, as shown in Fig. 4b, the total thickness of IMC layers gradually increased. A thin new IMC layer emerged between $(Cu,Ni)_6Sn_5$ and Cu, corresponding to $(Cu,Ni)_3Sn$ by EDS analysis. When the aging time was extended to 240 h and 480 h, as shown in Fig. 4c and d, interestingly, the total thicknesses of the IMCs layer were rapidly increased with the rising aging time. Moreover, the thickness of $(Cu,Ni)_6Sn_5$ layer seemed to grow rapidly, but the thickness of $(Cu,Ni)_3Sn$ layer seemed to keep constant.

3.2 Interfacial transfer of Sn–*x*/Cu joints

The total thicknesses of $(Cu,M)_6Sn_5$ and $(Cu,M)_3Sn$ layers for the four kinds of solder joints aged at different aging periods is shown in Fig. 5. It was seen that the thickness of total IMCs layer increased with the aging time. Cu addition (0.7%) and Ag addition (3.5%) seemed to slightly affect the total IMC thickness. However, as presented in Fig. 5a, the growth rate of total IMCs layer in Sn0.1Ni/Cu joint was much larger than those of Sn/Cu, Sn0.7Cu/Cu and Sn3.5Ag/Cu joints. In addition, the growth behaviors of both $(Cu,M)_6Sn_5$ and $(Cu,M)_3Sn$ layers were sensitive to the Sn0.7Cu, Sn3.5Ag and Sn0.1Ni solder. With the increase of aging time, as presented in Fig. 5b, the thickness of Cu_6Sn_5 layer in Sn/Cu joints was relatively stable. While, the thickness of $(Cu,M)_6Sn_5$ layer in Sn0.7Cu/Cu, Sn3.5Ag/Cu and Sn0.1Ni/Cu joints gradually increased, especially Ni addition (0.1%). For the thickness of $(Cu,M)_3Sn$ layer, as shown in Fig. 5c, it was seen that the thickness of $(Cu,M)_3Sn$ layer increased with the aging time. The growth rate of Cu_3Sn layer in Sn/Cu joint was larger than those of Sn/Cu, Sn0.7Cu/Cu and Sn3.5Ag/Cu joints. It suggested that Cu addition (0.7%), Ag addition (3.5%) and Ni addition (0.1%) promoted growth of the $(Cu,M)_6Sn_5$ layer, especially Ni addition, while trace Cu, Ag and Ni addition had the function in suppressing growth of the $(Cu,M)_3Sn$ layer. Yoon et al. [36] investigated the effects of Cu on interfacial

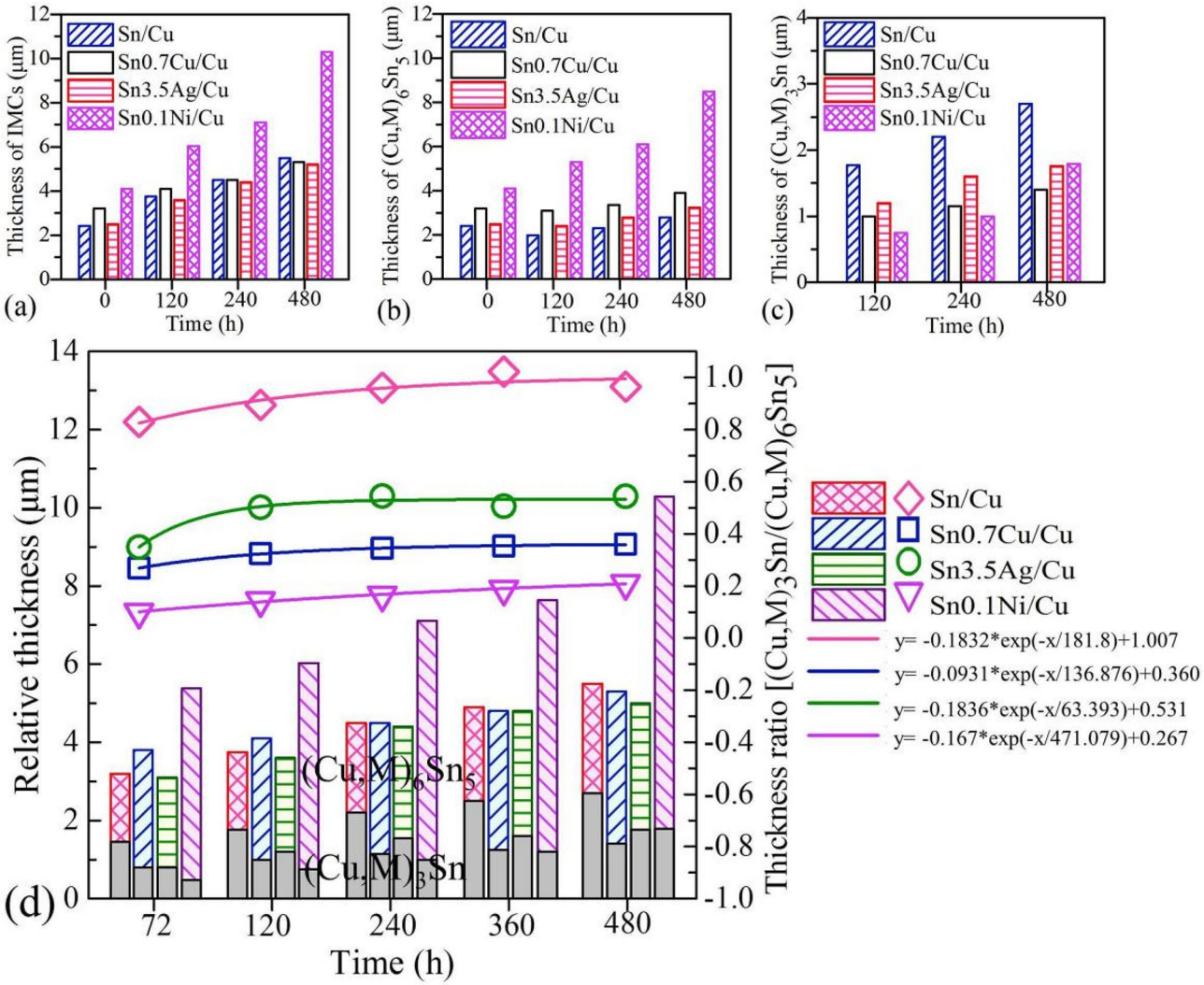

Fig. 5 **a** Average thickness of the IMCs layer with the thermal aging time, **b** thickness variation of the $(Cu,M)_6Sn_5$ (M = Cu, Ni) layer, **c** thickness variation of the $(Cu,M)_3Sn$ (M = Cu, Ni) layer, **d** thickness ratio of $(Cu,M)_3Sn$ to $(Cu,M)_6Sn_5$

reaction of Sn–Ag/Cu solder joints. They also found that increasing the amount of Cu in Sn–Ag solder significantly reduced the thickness of Cu_3Sn layer. In addition, Choi et al. [37] studied IMC growth in Sn–Ag/Cu solder joints. They found that the thickness ratio of Cu_6Sn_5 to Cu_3Sn was about 2:1 as aged at 150 °C for 700 h. In our previous work, the $(Cu,M)_6Sn_5/(Cu,M)_3Sn$ ratios were 1:1 in the Sn/Cu solder joint, 2.6:1 in the Sn0.7Cu/Cu, 1.7:1 in the Sn3.5Ag/Cu and 5:1 in the Sn0.1Ni/Cu as aged at 150 °C for 480 h. The results indicated that Cu, Ag and Ni were conducive to retard the growth of the $(Cu,M)_3Sn$ layer. Moreover, Cu and Ni had a more significant effect relative to Ag.

Figure 5d graphs the interfacial transfer (thickness ratio, y) of $(Cu,M)_3Sn/(Cu,M)_6Sn_5$ versus the thermal aging time (t). The interfacial transfer (thickness ratio, y) of the Sn−x/Cu joints was close to parabola relationship, $y = A \times \exp(-t/B) + C$, that was $y = -0.1889 \times \exp(-t/185.305) + 1.016$ for Sn/Cu joints, $y = -0.0924 \times \exp(-t/136.876) + 0.360$ for Sn0.7Cu/Cu joints, $y = -0.1925 \times \exp(-t/63.352) + 0.531$ for Sn3.5Ag/Cu joints and $y = -0.1701 \times \exp(-t/473.55) + 0.267$ for Sn0.1Ni/Cu joints, respectively. The results indicated that microelement addition was expected to change the $(Cu,M)_6Sn_5$ and $(Cu,M)_3Sn$ interfacial transfer at the Sn−x/Cu interface.

3.3 IMCs evolution of Sn−*x*/Cu joints

Cu_6Sn_5 phase was stable as the hexagonal structure η-Cu_6Sn_5 ($P6_3/mmc$) above 186 °C. When the temperature below 186 °C, the phase transition occurred, which transformed to a more stable crystalline, viz., the monoclinic structure η'-Cu_6Sn_5(C2/c) [38]. The solder joints were as-reflowed at

260 °C for 1 min at a temperature above 186 °C to form hexagonal phases η-Cu_6Sn_5. When the cooling rate was slow after as-reflowed, the hexagonal structure η-Cu_6Sn_5 part will be transformed into a monoclinic structure η'-Cu_6Sn_5. When the cooling rate was fast after as-reflowed, the hexagonal structure η-Cu_6Sn_5 will not change into a monoclinic structure η'-Cu_6Sn_5. Nogita et al. found that Ni (1–17.2 at.%) was doped in solder and was stable to the η-Cu_6Sn_5 phase after as-reflowed [39, 40]. Yang et al. show that Ni atoms can occupy the Cu2 sites in the η-Cu_6Sn_5 phases and this effect can prevent solder joints from forming the η'-Cu_6Sn_5 phases after as-reflowed cooling [41]. Figure 6 shows XRD phase analysis of the IMCs layers after as-reflowed and aging of Sn−*x*/Cu (*x* = 0, 0.7Cu, 3.5Ag and 0.1Ni) joints. The results shown that IMCs in Sn−*x*/Cu (*x* = 0, 0.7Cu and 3.5Ag) joints were η-$Cu_6Sn_5$and η'-Cu_6Sn_5 after as-reflowed and aging, respectively. In Sn0.1Ni/Cu joint, the IMC phase were η-$(Cu,Ni)_6Sn_5$ after as-reflowed and η'-$(Cu,Ni)_6Sn_5$ under aging.

The phase evolution of Sn−*x*/Cu (*x* = 0, 0.7Cu, 3.5Ag and 0.1Ni) joints and aging condition is summarized in Table 2. In the Sn−*x*/Cu (*x* = 0, 0.7Cu and 3.5Ag) joints, only η-Cu_6Sn_5, η'-Cu_6Sn_5 and ε-Cu_3Sn phases were only formed at the interface. As for Sn3.5Ag/Cu joint, the Ag_3Sn phase was also found both in the solder and at the interface. The interfacial phase of Sn0.1Ni/Cu joint was significantly different from that of Sn−*x*/Cu (*x* = 0, 0.7Cu and 3.5Ag) joints. The η-$(Cu,Ni)_6Sn_5$, η'-$(Cu,Ni)_6Sn_5$ and ε-$(Cu,Ni)_3Sn$ were formed at the interface of Sn0.1Ni/Cu joint. These results revealed that as the Ni element was added to the Sn solder,

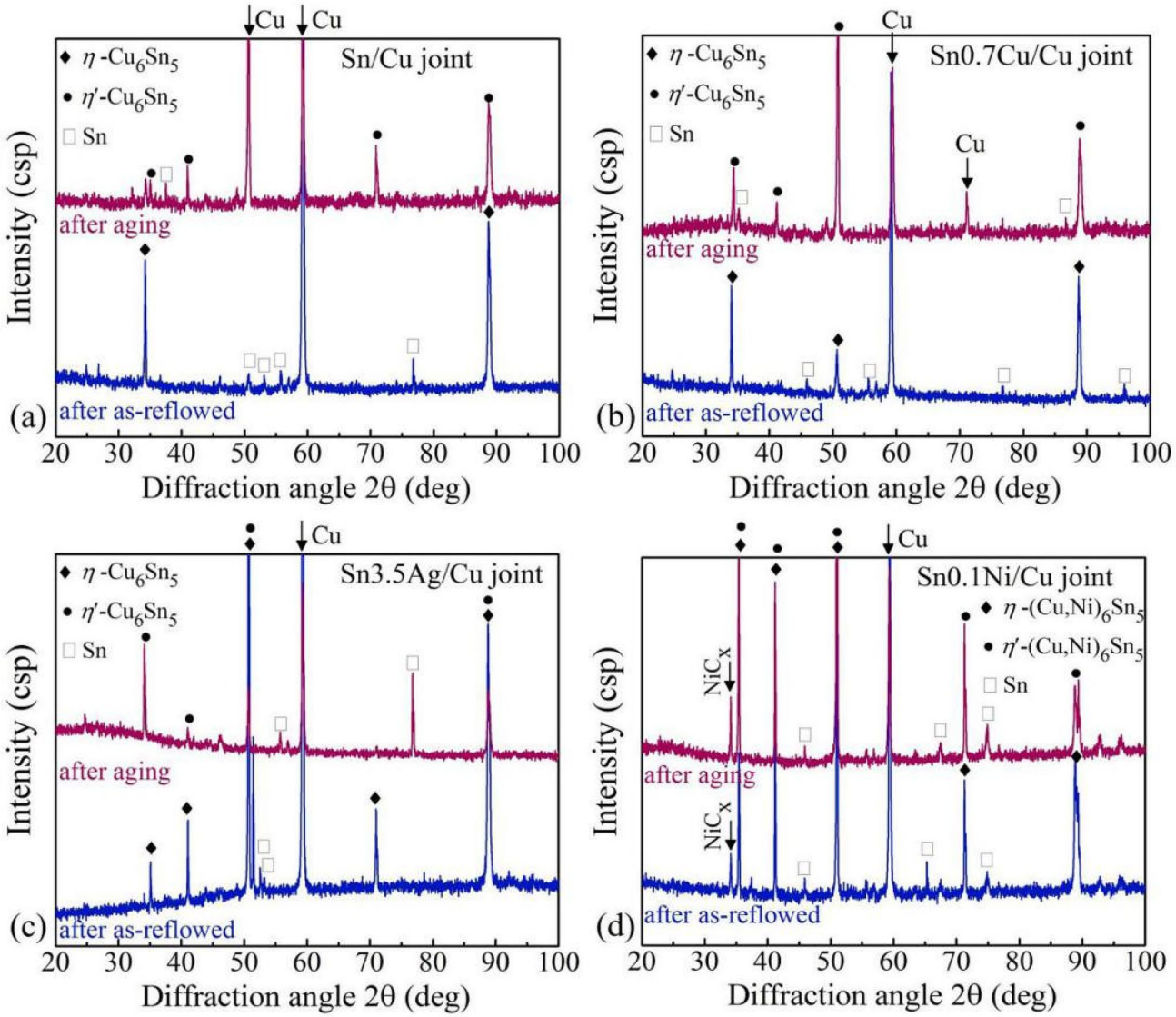

Fig. 6 XRD pattern of IMCs layer after as-reflowed and aging at 150 °C of **a** Sn/Cu, **b** Sn0.7Cu/Cu, **c** Sn3.5Ag/Cu and **d** Sn0.1Ni/Cu

Table 2 Phase evolution at Sn–*x*/Cu (*x* = 0, 0.7Cu, 3.5Ag and 0.1Ni) joints in following different thermal aging times

Solder joints	After as-reflowed at 260 °C	Aging time at 150 °C		
		120 h	240 h	480 h
Sn/Cu	η-Cu_6Sn_5	η'-Cu_6Sn_5 ε-Cu_3Sn	η'-Cu_6Sn_5 ε-Cu_3Sn	η'-Cu_6Sn_5 ε-Cu_3Sn
Sn0.7Cu/Cu	η-Cu_6Sn_5	η'-Cu_6Sn_5 ε-Cu_3Sn	η'-Cu_6Sn_5 ε-Cu_3Sn	η'-Cu_6Sn_5 ε-Cu_3Sn
Sn3.5Ag/Cu	Ag_3Sn η-Cu_6Sn_5	Ag_3Sn η'-Cu_6Sn_5 ε-Cu_3Sn	Ag_3Sn η'-Cu_6Sn_5 ε-Cu_3Sn	Ag_3Sn η'-Cu_6Sn_5 ε-Cu_3Sn
Sn0.1Ni/Cu	η-$(Cu,Ni)_6Sn_5$	η'-$(Cu,Ni)_6Sn_5$ ε-$(Cu,Ni)_3Sn$	η'-$(Cu,Ni)_6Sn_5$ ε-$(Cu,Ni)_3Sn$	η'-$(Cu,Ni)_6Sn_5$ ε-$(Cu,Ni)_3Sn$

the Ni atoms were incorporated into the Cu and Sn sublattice of the Cu–Sn IMCs, while the Ag element did not.

To understand the phase evolution of Sn–*x*/Cu joints by considering trace Cu, Ag and Ni, the optimized lattice parameters, lattice volumes (*V*) and formation enthalpy (ΔH_f), which provided a quantitative criterion for phase stability, were calculated. The results are listed in Table 3. It was found that the obtained lattice parameters and cell volumes for η-Cu_6Sn_5, η'-Cu_6Sn_5, ε-Cu_3Sn and Ag_3Sn were in good agreement with the available experimental results [35] and theoretical values [35, 42], where the deviations were less than 3%. As to Cu, the obtained lattice parameter and cell volume also agreed well with experimental results [43]. With respect to Ni, it had a face-centered cubic structure, while Sn had a tetragonal structure (β-Sn). The calculated bond length was close to the experimental results [44, 45].

The enthalpy of formation per atom was evaluated relative to the composition-averaged energies of the pure elements in their equilibrium crystal structures [46]. The enthalpy of formation (ΔH_f) for IMCs was expressed by the following equation:

$$\Delta H_f = [E^T - (mE_A^{solid} + nE_B^{solid} + lE_C^{solid})]/(m+n+l), \quad (1)$$

where E^T was the total energy of IMC $A_mB_nC_l$, (A, B, and C were the composition elements; *n*, *m*, and *l* were the number

Table 3 Structural properties obtained by GGA calculations, in comparison with other theoretical and experimental works

Phase	Method	Lattice parameters	V(Å^3)	ΔH_f (kJ/mol)
η'-Cu_6Sn_5	GGA[4×6×6] Exp. by others	$a=b=6.659$ Å $c=9.968$ Å $a=b=6.605$ Å $c=9.827$ Å	404.35 389.68 [35]	−6.63 −7.03 [35]
η-Cu_6Sn_5	GGA[4×6×6] Exp. by others	$a=b=4.188$ Å $c=5.110$ Å $a=b=4.198$ Å $c=5.096$ Å	77.61 77.78 [42]	−7.02
ε-Cu_3Sn	GGA[4×6×6] Exp. by others	$a=5.43$ Å, $b=4.31$ Å $c=4.66$ Å $a=5.490$ Å, $b=4.320$ Å $c=4.740$ Å	113.05 112.42 [43]	−8.52 −8.20 [44]
Ag_3Sn	GGA[4×6×6] Exp. by others	$a=6.080$ Å, $b=4.892$ Å $c=5.277$ Å $a=5.968$ Å, $b=4.780$ Å $c=5.184$ Å	153.98 147.89 [48]	−7.69 −7.81 [44]
Cu	GGA[8×8×8] Exp.by others	$a=b=c=3.629$ Å $a=b=c=3.615$ Å	47.79 47.23 [45]	Bond length
Ni	GGA[8×8×8] Exp.by others	a=b=c=3.554 Å a=b=c=3.524 Å	44.88 43.76 [49]	
β-Sn	GGA[4×4×8] Exp.by others	$a=b=c=6.670$ Å $a=b=c=6.491$ Å	296.72 273.51 [50]	

Lattice parameters *a* (Å), *b* (Å), *c* (Å); formation enthalpy ΔH_f (kJ/mol). Information in square brackets shows the final setting values for *k*-point meshes and their corresponding *k*-point numbers

of atoms), E_A^{solid}, E_B^{solid} and E_C^{solid} were the total energy per atom of A, B, and C crystals, respectively. The calculated results are summarized in Table 3. The ΔH_f of η-Cu_6Sn_5, η'-Cu_6Sn_5, ε-Cu_3Sn and Ag_3Sn were almost negative values, indicating that these binary IMCs were thermodynamic stable to be synthesized. It was seen that our results were nearly close to the reported results [35, 44] and our experimental phenomenon. Comparably, ε-Cu_3Sn had the lowest ΔH_f following by Ag_3Sn, η-Cu_6Sn_5 and η'-Cu_6Sn_5 had the highest ΔH_f.

For ternary η'-Cu_6Sn_5 and ε-Cu_3Sn based structures with Ni and Ag substitution, the calculated results are summarized in Table 4 and Fig. 7. The calculated ΔH_f of $(Cu,Ni)_6Sn_5$ and $(Cu,Ni)_3Sn$ were lower than those for Cu_6Sn_5 and Cu_3Sn, respectively. It indicated that the substitutional sites of Ni atom at Cu atoms occupation would increase the stability of Cu_6Sn_5 and Cu_3Sn. In addition, for the seven kinds of Ni doped Cu_6Sn_5 IMCs, $Cu_4Ni_2Sn_5$ (in which the Ni atom displaced the Cu at 8f site) had the minimum ΔH_f (-16.119 kJ/mol^{-1}) indicating that this IMCs was the most thermodynamically stable structure. Yang et al. [47] examined the additive elements on structural and electronic properties of Sn-based IMCs. Yu et al. [46] studied the structural and electronic properties of $Cu_{6-x}Ni_xSn_5$ ($x=0, 1, 2$) IMCs based on first principles. These research works reflected that Ni atom was favorably occupied the Cu2(8f) site of the Cu_6Sn_5 IMCs. Among the three kinds of Ni doped Cu_3Sn IMCs, the substitutional sites of Ni atom at Cu2(4f) was preferential occupation (e.g., $Cu_{2.5}Ni_{0.5}Sn$, -19.993 kJ/mol). However, the ternary structures with Ag element ($(Cu,Ag)_6Sn_5$ and $(Cu,Ag)_3Sn$) had higher ΔH_f than that of Ag_3Sn, it meant that binary Ag_3Sn IMCs was the more thermodynamically stable structure than that of ternary structures ($(Cu,Ag)_6Sn_5$ and $(Cu,Ag)_3Sn$). These calculated results agreed well with the experimental results in this work.

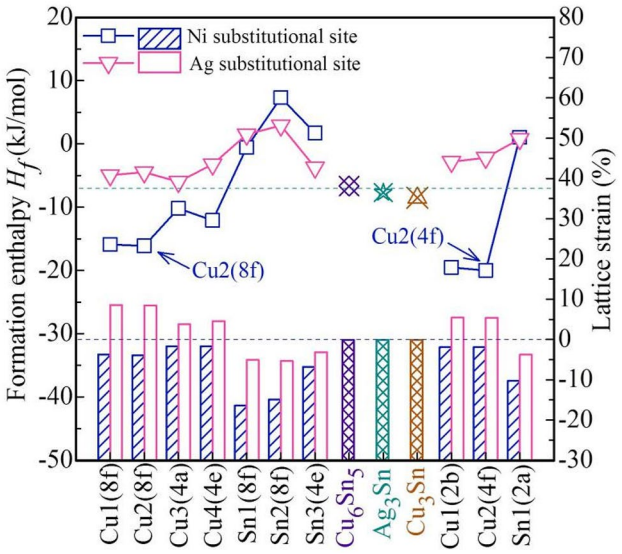

Fig. 7 Formation enthalpy (ΔH_f), and lattice strain varying with the substitutional site of Ni and Ag atom in η'-Cu_6Sn_5 and ε-Cu_3Sn based structure

The charge transfer of IMCs models considering Ni and Ag distribution is shown in Fig. 8. It was easy to found that the electron density difference distribution curve of IMCs layer after Ni doping greater than that of Cu_6Sn_5 and Cu_3Sn layer, that means more charge transfer of IMCs layer when Ni atoms were incorporated into the Cu and Sn sublattice of the Cu–Sn IMCs. The results were also visualized in the images of electron density difference (Fig. 8a, b illustration). It was seen that the blue regions near Ni atoms, which indicated that the charge transfer between Ni atom and neighboring Cu atoms. In other words, there

Table 4 Calculated formation enthalpy ΔH_f for the η'-Cu_6Sn_5, η-Cu_6Sn_5 and ε-Cu_3Sn based structures with Ni and Ag substitution (kJ/mol)

η'-Cu_6Sn_5 based	Substitutional site	ΔH_f(kJ/mol)	ε-Cu_3Sn based	Substitutional site	ΔH_f (kJ/mol)
$Cu_4Ni_2Sn_5$	Cu1(8f)	−15.905	$Cu_{2.5}Ni_{0.5}Sn$	Cu1(2b)	−19.540
$Cu_4Ni_2Sn_5$	Cu2(8f)	−16.119	$Cu_{2.5}Ni_{0.5}Sn$	Cu2(4f)	−19.993
Cu_5NiSn_5	Cu3(4a)	−10.208	$Cu_3Ni_{0.5}Sn_{0.5}$	Sn1(2a)	1.043
Cu_5NiSn_5	Cu4(4e)	−12.109			
$Cu_6Ni_2Sn_3$	Sn1(8f)	−0.557			
$Cu_6Ni_2Sn_3$	Sn2(8f)	7.314			
Cu_6NiSn_4	Sn3(4e)	1.729			
$Cu_4Ag_2Sn_5$	Cu1(8f)	−4.944	$Cu_{2.5}Ag_{0.5}Sn$	Cu1(2b)	−2.832
$Cu_4Ag_2Sn_5$	Cu2(8f)	−4.477	$Cu_{2.5}Ag_{0.5}Sn$	Cu2(4f)	−2.194
Cu_5AgSn_5	Cu3(4a)	−5.986	$Cu_3Ag_{0.5}Sn_{0.5}$	Sn1(2a)	0.798
Cu_5AgSn_5	Cu4(4e)	−3.244			
$Cu_6Ag_2Sn_3$	Sn1(8f)	1.508			
$Cu_6Ag_2Sn_3$	Sn2(8f)	2.913			
Cu_6AgSn_4	Sn3(4e)	−3.717			

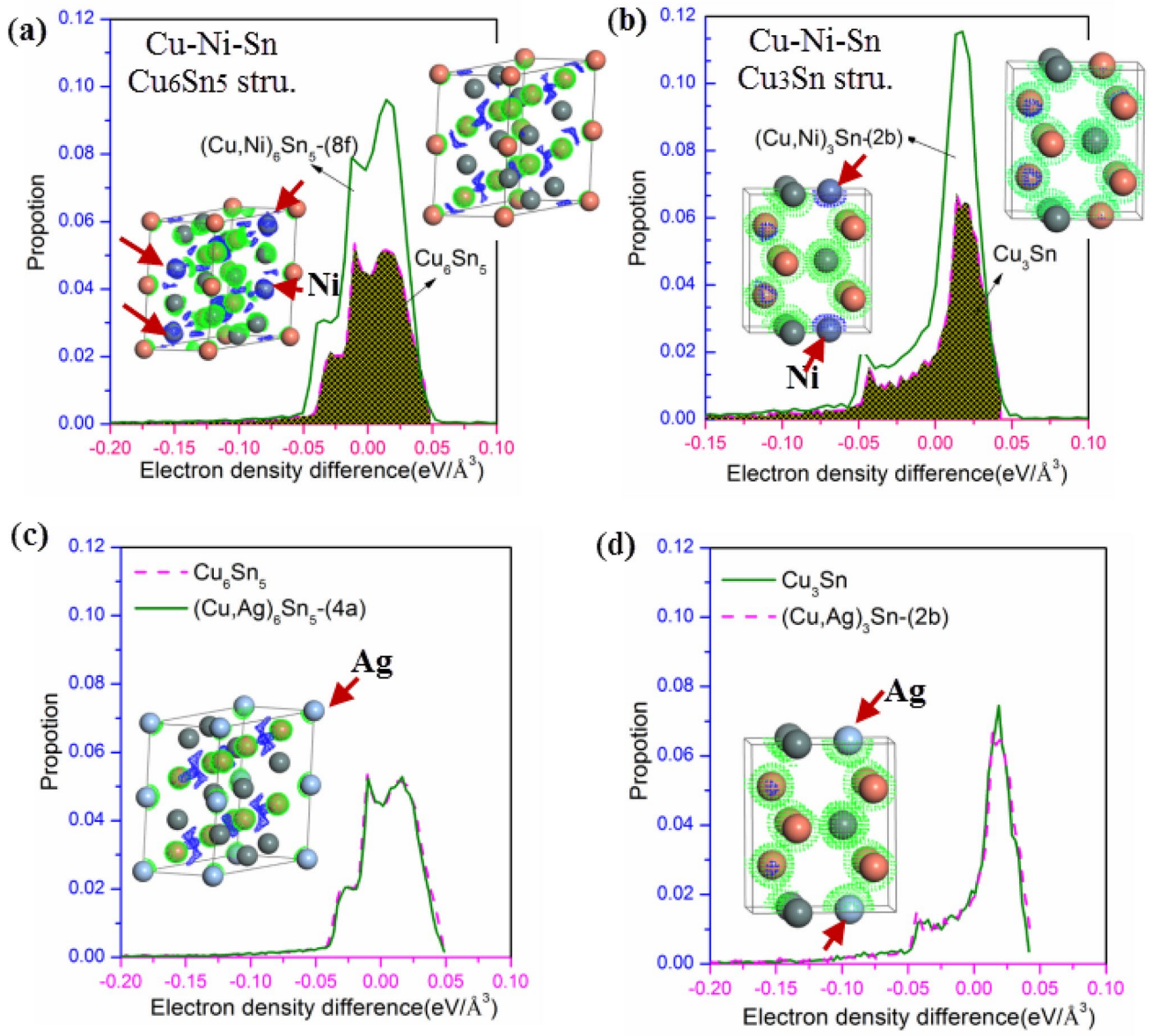

Fig. 8 Comparative figures of electron density difference of Cu–Sn layer, Cu–Ni–Sn layer (**a**, **b**) and Cu–Ag–Sn layer (**c**, **d**). The blue and green regions show regions of electron accumulation and loss

existed a stronger affinity between Cu and Ni in the case of Ni addition into the Cu–Sn system. From Fig. 7, it was also easy to obtain the fact that the lattice volume shrinkage of IMCs layers because of stronger affinity between Cu and Ni from Cu–Sn layer to Cu–Ni–Sn layer. However, for ternary Cu–Ag–Sn system, the electron density difference distribution curve of IMCs layer changed little from Cu–Sn layer to Cu–Ag–Sn layer (Fig. 8c, d). In addition, it was known that the atomic radius of Cu and Ag were 1.278 Å and 1.445 Å, respectively. It was difficult for large Ag atoms to replace small Cu atoms. Therefore, the Cu–Ag–Sn layer was not easy to form at the Sn3.5Ag/Cu interface.

4 Discussion

Atom flux partially controls an interfacial reaction, and the grain-boundary diffusion mechanism is a dominant diffusion mechanism in the Sn/Cu reaction couple [51, 52]. The coarser the grains, the fewer the existing grain boundaries, and therefore, the atoms would take longer time to diffuse through the barrier. The grain sizes of the Cu_6Sn_5 IMC layer are analyzed through the top image (as shown in Fig. 9). During thermal aging, the grain size of the Cu_6Sn_5 layers in the Sn/Cu joints is relatively coarser than that in the Sn-based/Cu joints. The mean grain size of the Cu_6Sn_5 layer in the pure Sn/Cu aged for 480 h is 4.49 μm, while those of top IMC layer in Sn0.7Cu/

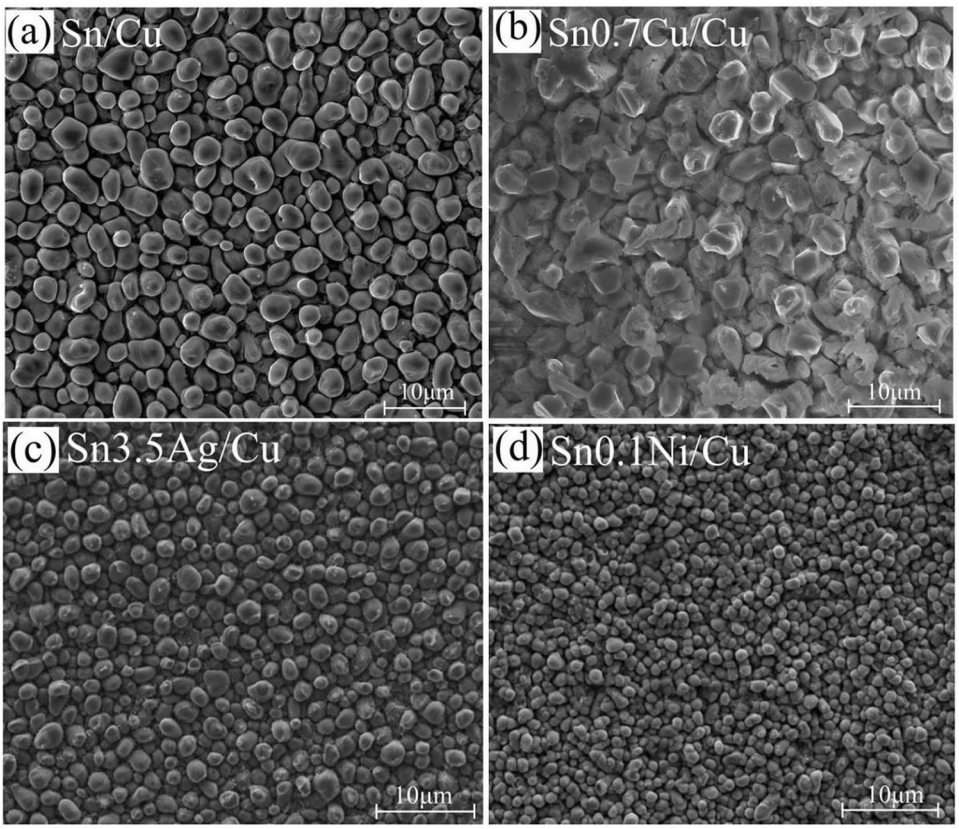

Fig. 9 Top-view images of as-reflowed **a** Sn/Cu, **b** Sn0.7Cu/Cu, **c** Sn3.5Ag/Cu and **d** Sn0.1Ni/Cu joints

Cu, Sn3.5Ag/Cu and Sn0.1Ni/Cu are 3.51 μm, 3.47 μm and 2.15 μm, respectively. The results indicate that the Cu, Ag and Ni addition could refine the grain of the top IMC layer.

For Sn–Cu system, the chemical reactions at Cu/Cu_3Sn and Cu_3Sn/Cu_6Sn_5 interfaces are represented by the chemical equations.

At the Cu/Cu_3Sn interface on the Cu_3Sn side (the elements in square brackets denote the diffusing species):

$$3Cu + [Sn] \rightarrow Cu_3Sn \tag{2}$$

At the Cu_3Sn/Cu_6Sn_5 interface on the Cu_3Sn side:

$$Cu_6Sn_5 + 9[Cu] \rightarrow 5Cu_3Sn \tag{3}$$

$$Cu_6Sn_5 \rightarrow 3[Sn] + 2Cu_3Sn \tag{4}$$

At the Cu_3Sn/Cu_6Sn_5 interface on the Cu_6Sn_5 side:

$$5Cu_3Sn \rightarrow 9[Cu] + Cu_6Sn_5 \tag{5}$$

$$2Cu_3Sn + 3[Sn] \rightarrow Cu_6Sn_5 \tag{6}$$

At the solder/Cu6Sn5 interface on the solder side:

$$6[Cu] + 5Sn \rightarrow Cu_6Sn_5 \tag{7}$$

According to the equations above, the interfacial reaction is a dynamic process. At the Cu_3Sn/Cu_6Sn_5 interface, the reaction direction in Eqs. (3) and (4) are opposite to that in Eqs. (5) and (6). The final reaction direction, i.e., the migration direction of the Cu_3Sn/Cu_6Sn_5 interface, is determined, to a large extent, by the diffusion fluxes of Cu and Sn. It is well known that copper was the dominant diffusing species in the Sn/Cu reaction couple [6]. We plot a sketch map reflecting the relation between interface behavior and Sn/Cu, Sn0.7Cu/Cu, Sn3.5Ag/Cu and Sn0.1Ni/Cu solder joints, respectively, based on the experimental results, as shown in Fig. 10. It is found that for the coarser Cu_6Sn_5 layer in Sn/Cu solder joints, a larger amount of Cu atoms would accumulate at the Cu_6Sn_5/Cu_3Sn interface due to less diffusion paths, promoting the growth of the Cu_3Sn layer by consuming Cu_6Sn_5 through the reaction Eq. (3). While for the finer $(Cu,M)_6Sn_5$ layer in Sn0.7Cu/Cu, Sn3.5Ag/Cu and Sn0.1Ni/Cu solder joints, the Cu atoms diffuse much quicker through the Cu_6Sn_5 layer. This was favorable for the reactions on the Cu_6Sn_5 side. Therefore, Cu_3Sn would transform to Cu_6Sn_5 through the reaction Eqs. (5) and (6).

In addition, as shown in Fig. 10b, doping the Cu element in the solder is likely to reduce the Cu concentration gradient at the solder/Cu interface, and suppress the diffusion of Cu atoms from Cu substrate to solder [53]. The declined Cu flux not only reduces the consumption of Cu substrate

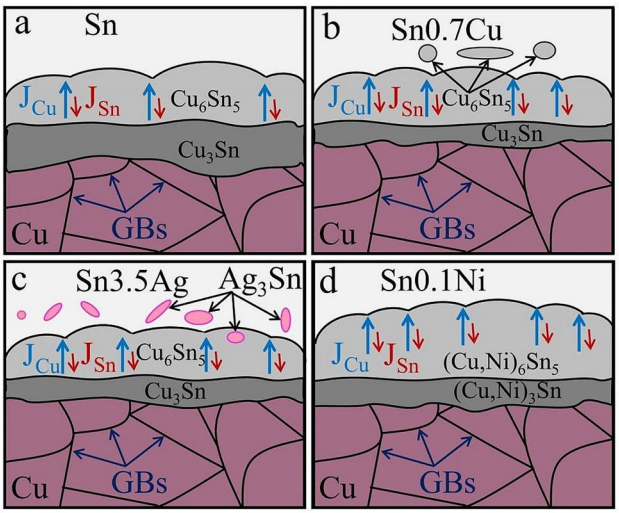

Fig. 10 Schematic illustration showing the general process for interfacial behavior in **a** Sn/Cu, **b** Sn0.7Cu/Cu, **c** Sn3.5Ag/Cu and **d** Sn0.1Ni/Cu

(Eq. 2), but also is favorable for the reactions on the Cu_6Sn_5 side (Eqs. 5 and 6). Therefore, the growth of Cu_3Sn layer is retard at both sides.

As shown in Figs. 3 and 10c, the addition of Ag causes the Ag_3Sn phases to form in the Sn3.5Ag solder. As the thermal aging time extends, Ag_3Sn phase gradually increases and embed in grain boundary of IMC layer, Ag_3Sn acts as a pinning effect, which divides the solder substrate into many regions, and suppress the inter-diffusion of Cu and Sn.

The addition of Ni causes the formation of $(Cu,Ni)_6Sn_5$ phases at the interface, the reaction of the chemical Eq. (8) occurs:

$$(6-x)\mathrm{Cu} + x\mathrm{Ni} + 5\mathrm{Sn} \rightarrow (\mathrm{Cu},\mathrm{Ni})_6\mathrm{Sn}_5 \quad (8)$$

As shown in Fig. 9d, the $(Cu,Ni)_6Sn_5$ layer are composes of multi-layer small size crystal grains. This kind of structure is beneficial to the inter-diffusion of Cu and Sn and the reactions of the Eqs. (6) and (7) occur. Besides, for the trace Ni containing joints, it seems that reaction $2(Cu,Ni)_3Sn + 3[Sn] \rightarrow (Cu,Ni)_6Sn_5$ dominates, because the Ni doping increases the stability of Cu_6Sn_5.

5 Conclusions

In this study, the interfacial transfer and phase evolution between Cu and Sn solder doped with minor Cu, Ag and Ni were investigated. The results were summarized as follows:

(1) After thermal aging at 150 °C, a layer of Cu_6Sn_5 and Cu_3Sn was observed in the joints of Sn/Cu, Sn0.7Cu/Cu and Sn3.5Ag/Cu; while it changed into $(Cu,Ni)_6Sn_5$ and $(Cu,Ni)_3Sn$ in the joint of Sn0.1Ni/Cu. Cu, Ag and Ni additions were able to suppress the growth of $(Cu,M)_3Sn$ (M = Cu, Ni) layers, but promoted the $(Cu,M)_6Sn_5$ growth.

(2) The interfacial transfer (thickness ratio, y) of $(Cu,M)_3Sn/(Cu,M)_6Sn_5$ versus the thermal aging time (t) was close to parabola relationship.

(3) For ternary Cu–Ni–Sn system, as the Cu sites were substituted by Ni, the volume of the cells shrinked and the distance between the atoms were shortened, which resulted in strengthening of bonding force between atoms. Moreover, the substitutional sites of Ni atom at Cu atoms occupation would increase the stability of Cu_6Sn_5 and Cu_3Sn. The preferential occupation of Ni in Cu_6Sn_5 and Cu_3Sn were Cu2(8f) and Cu2(4f) sites, respectively.

(4) The electron density difference distribution curve of IMCs layer changed little from Cu–Sn layer to Cu–Ag–Sn layer. Meanwhile, the atomic radius of Ag atom (1.445 Å) was larger than that of Cu atom (1.278 Å). It was difficult for large Ag atom to replace small Cu atom. Therefore, the Cu–Ag–Sn layer was not easy to form at the Sn3.5Ag/Cu interface.

(5) The grains size of IMC layer near the solder were refined by Cu, Ag and Ni, and it was beneficial in increasing atom diffusion through the $(Cu,M)_6Sn_5$ layer. This was favorable for the reactions on the Cu_6Sn_5 side. Therefore, $(Cu,M)_3Sn$ layer would transform to $(Cu,M)_6Sn_5$ layer.

Acknowledgements This project is supported by National Natural Science Foundation of China (Grant no. 51805316), China postdoctoral Science Foundation (No.2019M651491), Shanghai Science and Technology Committee Innovation Grant (17JC1400600 17JC1400601, 19511106400 and 19511106402). Karamay Science and Technology Major Project (2018ZD002B) and Aid for Xinjiang Science and Technology Project (2019E0235).

References

1. X.-Y. Zhao, M.-Q. Zhao, X.-Q. Cui, T.-H. Xu, M.-X. Tong, Trans. Nonferrous Met. Soc. China **17**, 805 (2007)
2. W. Yue, H.-B. Qin, M.-B. Zhou, X. Ma, X.-P. Zhang, Trans. Nonferrous Met. Soc. China **2014**(24), 1619 (2014)
3. F. Xing, X.-M. Qiu, Y.-D. Li, Trans. Nonferrous Met. Soc. China **25**, 879 (2015)
4. K.N. Tu, Y.-X. Liu, Mater. Sci. Eng. R **136**, 1 (2019)
5. Q.-Y. Yin, F. Gao, Z.-Y. Gu, J.-R. Wang, E.A. Stach, G.-W. Zhou, Acta Mater. **125**, 136 (2017)
6. J.-S. Chen, Y.-Z. Zhang, Z.-S. Yu, P.-L. Zhang, W.-Q. Zhao, J. Yang, D. Wu, Appl. Sci. **8**, 1 (2018)
7. S.M. Hayes, N. Chawla, D.R. Frear, Microelectron. Reliab. **49**, 269 (2015)

8. W.-H. Chen, C.-F. Yu, H.-C. Cheng, Y. Tsai, S.-T. Lu, Microelectron. Reliab. **53**, 30 (2013)
9. H.-F. Zou, H.-J. Yang, Z.-F. Zhang, Acta Mater. **56**, 2649 (2008)
10. M.-B. Zhou, X. Ma, X.-P. Zhang, J. Electron. Mater. **41**, 3169 (2012)
11. J. Yang, Z.-S. Yu, Y.-L. Li, H. Zhang, N. Zhou, Sci. Technol. Weld. Join. **23**, 543 (2018)
12. J. Yang, Y.-L. Li, P.-L. Zhang, C.S. Dulai, Z.-S. Yu, J. Mater. Process. Technol. **272**, 40 (2019)
13. C. Chen, H.Y. Hsiao, Y.-W. Chang, F. Ouyang, K.N. Tu, Mater. Sci. Eng. R **73**, 85 (2012)
14. Y.-X. Liu, Y.-C. Chu, K.N. Tu, Acta Mater. **117**, 146 (2016)
15. J.-S. Chen, J. Yang, Y.-Z. Zhang, Z.-S. Yu, P.-L. Zhang, Weld. World **63**, 751 (2019)
16. M.Y. Tsai, S.-C. Yang, Y.-W. Wang, C.-R. Kao, J. Alloy. Compd. **494**, 123 (2010)
17. J.-S. Chen, H.-K. Zhang, P.-L. Zhang, Z.-S. Yu, Y.-Z. Zhang, C. Yu, H. Lu, J. Mater. Res. Technol. **8**, 4141 (2019)
18. S.-Y. Zhang, X.-Y. Xu, T.-S. Lin, P. He, J. Mater. Sci. Mater. Electron. **30**, 13855 (2019)
19. F.-J. Wang, H. Chen, Y. Huang, L.-T. Liu, Z.-J. Zhang, J. Mater. Sci. Mater. El. **30**, 3222 (2019)
20. N. Zhao, M.-Y. Wang, Y. Zhong, H.-T. Ma, Y.-P. Wang, C.-P. Wong, J. Mater. Sci. Mater. Electron. **29**, 1 (2018)
21. C. Yu, J.-S. Chen, K.-Y. Wang, J.-Q. Chen, H. Lu, J. Mater. Sci. Mater. Electron. **24**, 4630 (2013)
22. H.T. Lee, Y.-F. Chen, J. Alloy Compd. **509**, 2510 (2011)
23. H.W. Tseng, C.-Y. Liu, Mater. Lett. **62**, 3887 (2008)
24. F.-L. Zhu, H.-H. Zhang, R.-F. Guan, S. Liu, J. Alloy. Compd. **438**, 100 (2007)
25. Y.-W. Wang, C.-C. Chang, C.-R. Kao, J. Alloy. Compd. **478**, L1 (2009)
26. K.-J. Zeng, R. Stierman, T.-C. Chiu, D. Edwards, K. Ano, K.N. Tu, J. Appl. Phys. **97**, 1 (2005)
27. T.T. Mattila, J. Hokka, K.M. Paulasto, J. Electron. Mater. **43**, 4090 (2014)
28. J.-S. Chen, C.-H. Ye, J.-M. Chen, J.-J. Xu, C. Yu, H. Lu, Mater. Lett. **161**, 201 (2015)
29. S.J. Clark, M.D. Segall, C.J. Pickard, P.J. Hasnip, M.I.J. Probert, K. Refson, M.C. Payne, Z. Krist. **220**, 567 (2005)
30. J.P. Perdew, K. Burke, M. Ernzerhof, Phys. Rev. Lett. **77**, 3865 (1996)
31. D. Vanderbilt, Phys. Rev. B **41**, 7892 (1990)
32. D.J. Chadi, Phys. Rev. B **16**, 1746 (1977)
33. H.K. Kim, K.N. Tu, Phys. Rev. B **53**, 16027 (1996)
34. M. Yang, M.-Y. Li, L. Wang, Y.-G. Fu, J.-Y. Kim, L.-Q. Weng, J. Electron. Mater. **40**, 176 (2011)
35. G. Ghosh, M. Asta, J. Mater. Res. **20**, 3102 (2005)
36. J.W. Yoon, B.I. Noh, S.B. Jung, J. Alloy. Compd. **506**, 331 (2010)
37. S. Choi, T.R. Bieler, J.P. Lucas, K.N. Subramanian, J. Electron. Mater. **28**, 1209 (1999)
38. K. Nogita, C.M. Gourlay, S.D. Mcdonald, Y.Q. Wu, J. Read, Q.F. Gu, Scripta Mater. **65**, 922 (2011)
39. K. Nogita, T. Nishimura, Scripta Mater. **59**, 191 (2008)
40. Y.Q. Wu, S.D. Mcdonald, J. Read, H. Huang, K. Nogita, Scripta Mater. **68**, 595 (2013)
41. W.-H. Yang, Y. Tomokazu, A. Kohei, S. Flora, K. Nogita, M. Syo, Scripta Mater. **158**, 1 (2019)
42. W. Arne, P. Gösta, Z. Anorg, Allg. Chem. **175**, 80 (1928)
43. W. Burkhardt, K. Schubert, Z Metallkd. **50**, 442 (1959)
44. H. Flandorfer, U. Saeed, C. Luff, A. Sabbar, H. Ipser, Thermochim. Acta **459**, 34 (2007)
45. M.H. Otte, J. Appl. Phys. **32**, 1536 (1961)
46. C. Yu, J.-Y. Liu, H. Lu, P.-L. Li, J.-M. Chen, Intermetallics **15**, 1471 (2007)
47. C. Yu, J.-S. Chen, J.-J. Xu, J.-M. Chen, H. Lu, Mater. Res. Express **1**, 025702 (2014)
48. C.W. Fairhurst, J.B. Cohen, Acta Crystallogr. Sec. B **28**, 371 (1972)
49. J. Haglund, G.A. Fernandez, G. Grimvall, M. Korling, Phys. Rev. B **48**, 11685 (1993)
50. V.T. Deshpe, D.B. Sirdeshmukh, Acta Crystallogr. **15**, 294 (2010)
51. S. Kim, J. Yu, Scripta Mater. **67**, 312 (2012)
52. K. Jung, H. Conrad, J. Mater. Sci. **42**, 3994 (2007)
53. Y.-W. Wang, Y.-W. Lin, C.-R. Kao, J. Alloy Compd. **493**, 233 (2010)